LASER HEATING AND THERMAL STRESSES TIME EXPONENTIALLY HEATING PULSE CASE

B.S. Yilbas and I. Z. Naqvi
King Fahd University of Petroleum & Minerals (KFUPM)
Mechanical Engineering Department
Dhahran, Saudi Arabia
Contact: bsyilbas@kfupm.edu.sa

Received June 2005, Accepted March 2006
No. 05-CSME-23, E.I.C. Accession 2875

ABSTRACT

Model studies of laser heating process minimize the experimental time and cost and give insight into the laser workpiece interaction mechanism. In the present study laser pulse heating is modelled and the governing equation of heat transfer, including phase change process, and thermal stresses are solved numerically using a control volume approach. In order to account for the time variation of the laser heating pulse, time exponentially varying pulse intensity is employed in the analysis. Since the heating conditions are considered to be axisymmetric, two dimensional case is introduced in the analysis. The temperature and stress fields are simulated for steel. It is found that temperature level attains considerably high values in the melt zone and pulse parameter (β/γ) with small values (1/2) results in large evaporated zones. Equivalent stress level increases rapidly in the region close to the melt surface and two stress peaks are developed in the radial direction. The location of stress peaks remains same with progressing heating period; however, the magnitude of second peak reduces with advancing heating periods.

ECHAUFFEMENT PAR LASER ET CONTRAINTES THERMIQUES : CAS DE VARIATION EXPONENTIELLE DE L'IMPULSION AVEC LE TEMPS

RESUME

La modélisation du procède de chauffage par laser aide a minimiser le coup et le temps d'expérimentation. La présente étude traite de la modélisation du procédé de chauffage par impulsion de laser. L'équation de la chaleur, le procède de changement de phase ainsi que les contraintes thermiques sont résolues par la méthode numérique en utilisant la technique du volume de contrôle. La variation avec le temps du chauffage par impulsion est prise en considération en faisant varier l'intensité de l'impulsion exponentiellement avec le temps. Etant donné la nature axisymétrique du problème l'analyse bidimensionnelle est adoptée pour l'acier. Les résultats montrent que la température est très élevée dans la zone au le matériau s'est écoulé. Le paramètre (β/γ) avec les petites valeurs de (1/2) conduit a de grandes zones d'évaporation du matériau. La valeur de la contrainte équivalente augmente rapidement autours de la zone d'écoulement. La contrainte radiale montre deux maxima dans cette zone. La position de ces maxima est indépendante du temps d'échauffement mais la valeur du deuxième sommet est réduite avec les longues périodes échauffement.

1 INTRODUCTION

Laser processing of materials finds wide application in industry due to its precise of operation, low cost and rapid processing. Laser processing of solid substrate falls into two categories, namely conduction-limited and non-conduction limited heating situations. In the conduction limited heating case, substrate material is heated to its melting temperature while phase change, including melting and evaporation, is involved with non-conduction limited heating. Therefore, laser heat treatment process falls into conduction limited heating while drilling, cutting and welding are non-conduction limited processes. Due to the several affecting parameters, process optimization through experimentation is lengthy and expensive. Consequently, modeling of the laser heating process reduces the duration of experiment and minimizes the experimental cost.

Considerable research studies have been carried out to explore the laser heating process analytically as well as numerically. Ready [1] introduced an analytical solution for laser step input pulse heating process. Analysis of heat conduction in deep penetration welding with time modulated laser beam was investigated by Simon et al [2]. They indicated that the time modulated laser beam had little effect on the resulting heat effected zone. Square-shaped laser beam heating of metallic substrate was studied by Lu [3]. He showed that the square shape of temperature profile was almost of the same size of the incident beam profile. Laser heating of a two-layer system was examined by El-Adawi et.al [4]. They used a Laplace transformation method to obtain the temperature distribution in two-layer system. Laser melting of metallic substrates was studied by Basu and Date [5]. They considered the marangoni effect in the melt pool when formulating the momentum and energy equations. They showed that two counter-rotating cells in the molten pools were resulted and the strength of circulation cells were dependent on the Prandtl number. Energy transfer rates and penetration velocity during a high-energy drilling process were investigated by Wei and Ho [6]. They indicated that the conventional one-dimensional penetration model was inherently invalid due to a significant overestimation of the evaporation rate. Multiple reflection and beam guiding during laser machining were analyzed numerically by Bang and Modest [7]. They indicated that multiple reflection resulted in increased material removal rates and deeper grooves, accompanied by a flatter profile near the centerline and steeper slopes in the other parts of the groove cross section. A study of thermal behavior and fluid flow during laser surface heating of alloys was carried out by Kim and Sim [8]. They indicated that convection in the mushy zone plays an important role in heat transfer and fluid flow during laser melting process. Yilbas and Shuja [9] investigated heat transfer characteristics of laser heated metallic surfaces. They introduced an equilibrium time for the heating process and indicated that for a given material, the balance occurred between the internal energy gain due to laser irradiation and the conduction losses. An analytical solution for surface ablation due to laser pulse heating was obtained by Yilbas and Al-Garni [10]. They found that as the heating progresses, the drilling velocities raised while the liquid depth and time to reach steady state reduced, in this case, the energy consumed for evaporation became higher than the diffusional losses towards the solid bulk. Moreover, laser heating mechanism including evaporation process initiating laser drilling was examined by Yilbas et al. [11]. They introduced analytical expression

for the drilling efficiency and validated their predictions through experimental results.

When the surface of the metallic substrate is heated by a laser beam, high temperature gradient is developed in the region irradiated by a laser beam, which in turn results in excessive stress levels in this region. Considerable research studies were carried out to explore the thermal stresses generated in the region heated by a laser beam. Paek and Gagliano [12] introduced an analytical solution to laser heating pulse and modelled the thermal stresses in the region next to cavity. Their solution was limited to surface heat source model, which did not represent accurately the laser heating process. Thermoelasticity problem for a multilayer coating-substrate heated by a laser beam was examined by Elperin and Rudin [13]. They developed an analytical expression for the temperature and stress fields and indicated that inelastic deformation occurred in the coating assembly even small temperature rise was resulted across the coating and the base substrate. A thermal stress development in the surface vicinity of steel due to laser irradiation was studied by Wang et al. [14]. The effects of phase transformation on the temperature rise and stress generation were investigated. They showed that laser quenching was the result of residual stress development in the surface vicinity of the substrate material during the cooling period. A plane stress model for fracture of ceramics during laser cutting process was introduced by Li and Sheng [15]. They showed that avoidance of fracture initiation resulted from a high energy laser beam cutting conditions. The thermal stresses and distortion gap width during laser welding were studied by Dain et al. [16]. The distortion of the unwelded section for the case of the infinite plate was compared with that for a thin plate of finite size computed by a finite element method. They indicated that the predictions agreed with the experimental results in acceptable limits. Yilbas et al [17] investigated thermal stresses due to laser pulse heating process. They showed that excessive stress levels were generated in the surface region of the substrate material.

The actual laser output pulse varies with time and when modelling the laser heating process, temporal variation of the laser pulse intensity should be incorporated in the analysis. Yilbas [18] introduced an exponential function resembling the actual laser pulse intensity, in which case, time exponentially varying pulse shape is employed. In the present study, laser heating of steel is considered. The Fourier heating model including phase change processes (melting and evaporation) is employed for time exponentially varying laser heating process. Thermal stresses in the solid material heated by a laser beam is also modelled. Temperature and stress fields are computed numerically using a control volume approach.

2 MATHEMATICAL ANALYSIS OF HEATING PROCESS

The heat transfer analysis employing a phase change process in the region irradiated by an intensity time exponentially varying laser pulse and thermal stresses developed in the solid phase of the substrate material due to the temperature field are presented. The analysis related to heat transfer and thermal stress field are given below.

2.1 Analysis of Heating Process

The Fourier heating model over estimates the lattice site temperature rise when the laser workpiece interaction time is comparable to the thermalization time of the substrate material ($\sim 10^{-12}$ s), in which case the non-equilibrium energy transport dominates over the heating process, which in turn results in electron temperature well excess of lattice site temperature occurs in the surface region of the substrate material [19]. On the other hand, the Fourier theory of heating becomes appropriate for laser pulse heating applications as the heating period extends to nanoseconds, i.e. electron and lattice site temperatures become identical [20].

In the analysis, a Gaussian power intensity distribution of a laser beam with its spot center at the center of the co-ordinate system is considered (figure (1.a)). This gives rise to an axisymmetric heating of the substrate material. Moreover, time exponentially varying laser beam intensity profile is employed to resemble the laser actual pulse [18]. When the temperature reaches to phase change temperatures of the substrate material (melting and evaporation temperatures) during the heating process, the phase change occurs, in which case the melting and subsequent evaporation of solid substrate are introduced in the governing equation of energy transport. In the case of solid phase heating, the conduction equation with insulated boundary condition at the surface is considered. The transient heat conduction equation for a substrate material irradiated by a laser beam with a Gaussian intensity profile and time exponentially varying pulse can be written as:

$$\rho_s c_{p_s} \frac{\partial T}{\partial t} = \frac{k_s}{r}\frac{\partial}{\partial r}\left(r\frac{\partial T}{\partial r}\right) + k_s\frac{\partial^2 T}{\partial z^2} + S_o \tag{1}$$

where,

$$S_o = I_o\delta\,(1-r_f)\,[\exp(-\beta t) - \exp(-\gamma t)]\exp(-\delta z)\exp\left(-\frac{r^2}{a^2}\right)$$

Io, δ, r_f, and a are the power intensity, absorption coefficient, surface reflectivity and the Gaussian parameter, respectively while β and γ are time exponentially varying pulse parameters.

The initial condition appropriate to equation 1 is:

$$\text{At time zero} \Rightarrow t = 0 \rightarrow T(r,z,0) = T_o \text{ (specified)}$$

The boundary conditions are:

$$\begin{aligned}
z \text{ at infinity} &\Rightarrow z = \infty \rightarrow T(r,\infty,t) = T_o \text{ (specified)}\\
r \text{ at infinity} &\Rightarrow r = \infty \rightarrow T(\infty,z,t) = T_o \text{ (specified)}\\
\text{At symmetry axis} &\Rightarrow r = 0 \rightarrow \frac{\partial T(0,z,t)}{\partial r} = 0\\
\text{At the surface} &\Rightarrow z = 0 \rightarrow \frac{\partial T(r,0,t)}{\partial z} = 0
\end{aligned}$$

In the case of phase change process, it is assumed that the substrate material has single melting and boiling temperatures, i.e., when the substrate material reaches the

melting or evaporation temperatures, the phase change takes place at a constant temperature. To describe the energy transfer during a phase change process, an energy or enthalpy methods can be used. In this case of enthalpy method, the governing equation of energy transport can be written in terms of enthalpy equation [21] as given in appendix 1. Moreover, once the phase change occurs, a mushy zone (partially solid and partially liquid or partially liquid and partially vapor) is generated across the region where the phase change takes place (figure (1.b)). Consequently, when formulating the phase change problem, the consideration is given for the generation of a mushy zone. In this case, during the phase change process, temperature of the substrate material remains same, but its enthalpy changes. In order to formulate the problem the following approach is introduced, namely an energy method. Consider a differential element in a substrate material (figure (1.b)), which is subjected to a melting process and let x_m is the mass fraction of liquid present in the element, then the energy content (ΔU) of the differential element with volume ΔV at melting temperature T_m can be written as:

$$\Delta U = \rho_m \Delta V \left[x_m \left(L_m + c_{p_m} \left(T_m - T_{ref} \right) \right) + c_{p_s} \left(1 - x_m \right) \left(T_m - T_{ref} \right) \right]$$

where

$$x_m = \frac{m_m}{m_m + m_s}$$

T_{ref}, x_m, m_m, m_s are reference temperature for enthalpy, quality of liquid, mass of liquid and mass of solid in the element, respectively. After assuming specific heat of melt is the same as solid at melting temperature ($Cp_s = Cp_m$ at $T = T_m$), then above equation reduces to:

$$\Delta U = \rho_m \Delta V \left[x_m L_m + c_{p_m} \left(T_m - T_{ref} \right) \right]$$

For a unit volume, it reduces to:

$$\frac{\Delta U}{\Delta V} = \Delta u = \rho_m \left[x_m L_m + c_{p_m} \left(T_m - T_{ref} \right) \right]$$

Differentiation with time yields:

$$\frac{\partial u}{\partial t} = \rho_m L_m \frac{\partial x_m}{\partial t} \tag{2}$$

since $c_{p_m} \left(T_m - T_{ref} \right) = \text{const.}$

Substituting equation 2 into equation 1 gives the energy equation for the differential element subjected to a phase change process:

$$\rho_m L_m \frac{\partial x_m}{\partial t} = \frac{k_m}{r} \frac{\partial}{\partial r} \left(r \frac{\partial T}{\partial r} \right) + k_m \frac{\partial^2 T}{\partial z^2} + S_o \tag{3}$$

Equation 3 is applicable for the differential elements (cells defined by nodes in the substrate material) when temperature becomes melting temperature of the substrate material ($T = T_m$) and $0 \leq x_m \leq 1$, i.e., a mushy zone. Consequently, temperature of the cells with $0 \leq x_m \leq 1$ is set to melting temperature ($T = T_m$). When the value

of x_m exits 1 ($x_m > 1$) equation 3 is not applicable for the differential element under consideration. In this case, equation 1 is used to determine the temperature rise in the liquid heating with the liquid thermal properties employed, i.e., the liquid heating initiates and continues till the boiling point is reached.

In the case of boiling point is reached, the mushy zone consideration needs to be implemented. In this case, equation 3 can be modified for a differential element, which is subjected to the boiling, i.e.:

$$\rho_b L_b \frac{\partial x_b}{\partial t} = \frac{k_b}{r}\frac{\partial}{\partial r}\left(r\frac{\partial T}{\partial r}\right) + k_b\frac{\partial^2 T}{\partial z^2} + S_o \tag{4}$$

Equation 4 is applicable for the range $T = T_b$ and $0 \leq x_b \leq 1$ in the mushy zone (partially liquid partially vapor zone). Consequently, temperature of the cells with $0 \leq x_b \leq 1$ is set to boiling temperature ($T = T_b$). It should be noted that x_m is replaced with x_b, which represents the fraction of vapor phase in the differential element.

The boundary condition at the evaporating surface is introduced in relation to equation 4. In this case, the temperature along the evaporated surface is kept at boiling temperature, i.e., the cells in the evaporated region are kept at boiling temperature, i.e.:

$$\text{At } z = z_b \rightarrow T(r, z_b, t) = T_b$$

where z_b represents the axial location at the evaporated surface.

Equations 3 and 4 determine the relative position of solid-liquid and liquid-vapor interface in the substrate material. Liquid-vapor interface determines the shape and size of cavity generated after evaporation process.

Equations 1, 3, and 4 can be non-dimensionlized through introducing the following dimensionless parameters:

$$\begin{aligned}
r^* &= r\delta \\
z^* &= z\delta \\
a^* &= a_i\delta \\
t^* &= \alpha_i\delta^2 t \\
\beta^* &= \frac{\beta}{\alpha_i\delta^2} \\
\gamma^* &= \frac{\gamma}{\alpha_i\delta^2} \\
T^* &= \frac{Tk_o\delta}{I_o(1-r_f)}
\end{aligned}$$

where k_o represents the thermal conductivity at standard temperature. After introducing the dimensionless parameters, equations 1, 3 and 4 yield:

$$\frac{\partial T^*}{\partial t^*} = \frac{1}{r^*}\frac{\partial}{\partial r^*}\left(r^*\frac{\partial T^*}{\partial r^*}\right) + \frac{\partial^2 T^*}{\partial z^{*2}} + [\exp(-\beta^* t^*) - \exp(-\gamma^* t^*)]\exp(-z^*)\exp\left(-\frac{r^{*2}}{a^{*2}}\right) \tag{5}$$

$$\frac{\alpha_m \delta \rho_m L_m}{I_o(1-r_f)} \frac{\partial x_m}{\partial t^*} = \frac{1}{r^*} \frac{\partial}{\partial r^*} \left(r^* \frac{\partial T^*}{\partial r^*} \right) + \frac{\partial^2 T^*}{\partial z^{*2}} + [\exp(-\beta^* t^*) - \exp(-\gamma^* t^*)] \exp(-z^*) \exp\left(-\frac{r^{*2}}{a^{*2}}\right) \tag{6}$$

$$\frac{\alpha_b \delta \rho_b L_b}{I_o(1-r_f)} \frac{\partial x_b}{\partial t^*} = \frac{1}{r^*} \frac{\partial}{\partial r^*} \left(r^* \frac{\partial T^*}{\partial r^*} \right) + \frac{\partial^2 T^*}{\partial z^{*2}} + [\exp(-\beta^* t^*) - \exp(-\gamma^* t^*)] \exp(-z^*) \exp\left(-\frac{r^{*2}}{a^{*2}}\right) \tag{7}$$

The non-dimensional initial condition for equations 5, 6, and 7 are:

$$\text{At time zero} \Rightarrow t^* = 0 \rightarrow T^*(r^*, z^*, 0) = \frac{T_o}{I_o(1-r_f)/k_o\delta} \text{ (specified)}$$

The non-dimensional boundary conditions are:

$$z^* \text{ at infinity} \Rightarrow z^* = \infty \rightarrow T^*(r^*, \infty, t^*) = \frac{T_o}{I_o(1-r_f)/k_o\delta} \text{ (specified)}$$

$$r^* \text{ at infinity} \Rightarrow r^* = \infty \rightarrow T^*(\infty, z^*, t^*) = \frac{T_o}{I_o(1-r_f)/k_o\delta} \text{ (specified)}$$

$$\text{At symmetry axis} \Rightarrow r^* = 0 \rightarrow \frac{\partial T^*(0, z^*, t^*)}{\partial r^*} = 0$$

$$\text{At the surface} \Rightarrow z^* = 0 \rightarrow \frac{\partial T^*(r^*, 0, t^*)}{\partial z^*} = 0$$

Temperature distribution inside the substrate material is obtained solving the equations 5, 6, and 7 with the appropriate temperature ranges and boundary conditions.

2.2 Stress Analysis

After assuming no external forces are acting to the surface of the substrate material, the equation governing the thermal stresses due to laser pulse heating can be written after assuming the plain strain state, in cylindrical co-ordinates, as [22]:

$$\varepsilon_r = \frac{1}{E}[\sigma_r - \nu(\sigma_\theta + \sigma_z)] + \alpha_T T \tag{8}$$

$$\varepsilon_\theta = \frac{1}{E}[\sigma_\theta - \nu(\sigma_r + \sigma_z)] + \alpha_T T \tag{9}$$

$$\varepsilon_z = \frac{1}{E}[\sigma_z - \nu(\sigma_r + \sigma_\theta)] + \alpha_T T \tag{10}$$

where E, ν, and α_T are elastic module, Poisson's ratio, and thermal expansion coefficient, respectively.

Since the case is axisymmetry, the stress function can be defined when formulating the thermal stresses [22], i.e:

$$\sigma_r = \frac{\varphi}{r} \tag{11}$$

$$\sigma_\theta = \frac{d\varphi}{dr} \tag{12}$$

In case of plane strain, strain in the z-axis reduces to $\varepsilon_z = 0$ and σ_z can be determined from equation 10, i.e.:

$$\sigma_z = \nu\left(\sigma_r + \sigma_\theta\right) - \alpha_T E T \tag{13}$$

The compatibility equation for the rotationally symmetric case is [12]:

$$r\left(\frac{d\varepsilon_\theta}{dr}\right) + \varepsilon_\theta - \varepsilon_r = 0 \tag{14}$$

Substituting equations 8 -13 into equation 14, yields:

$$\frac{d^2\varphi}{dr^2} + \frac{1}{r}\frac{d\varphi}{dr} - \frac{\varphi}{r^2} = -\frac{\alpha_T E}{1-\nu}\frac{dT}{dr} \tag{15}$$

Integration of equation 15 becomes:

$$\varphi = -\left(\frac{\alpha_T E}{1-\nu}\right)\frac{1}{r}\int_{r_g}^{r} Trdr + \frac{C_1 r}{2} + \frac{C_2}{r} \tag{16}$$

since $\sigma_r = \frac{\varphi}{r}$, then σ_r yields:

$$\sigma_r = -\left(\frac{\alpha_T E}{1-\nu}\right)\frac{1}{r^2}\int_{r_g}^{r} Trdr + \frac{C_1}{2} + \frac{C_2}{r^2} \tag{17}$$

The boundary conditions for σ_r are:

$$\begin{aligned} \text{At the solid liguid interface} &\Rightarrow r = r_g \rightarrow \sigma_r = 0 \\ \text{At infinity} &\Rightarrow r \rightarrow \infty \rightarrow \sigma_r = 0 \end{aligned}$$

Introducing the boundary conditions into equation 13, the coefficients C_1 and C_2 becomes zero, i.e.

$C_1 = 0$ and $C_2 = 0$. Hence equation 13 reduces to:

$$\sigma_r = -\left(\frac{\alpha_T E}{1-\nu}\right)\frac{1}{r^2}\int_{r_g}^{r} Trdr \tag{18}$$

$$\sigma_\theta = -\left(\frac{\alpha_T E}{1-\nu}\right)\frac{1}{r^2}\left[\int_{r_g}^{r} Trdr - Tr^2\right] \tag{19}$$

$$\sigma_z = -\left(\frac{\alpha_T E}{1-\nu}\right)T \tag{20}$$

Introducing the dimensionless stress as:

$$\sigma^* = \sigma \left[\frac{1-\nu}{\alpha_T E}\right] \left[\frac{k\delta}{I_o(1-r_f)}\right]$$

The dimensionless thermal stresses becomes:

$$\sigma_r^* = -\frac{1}{r^{*2}} \int_{r_{g^*}}^{r^*} T^* r^* dr^* \tag{21}$$

$$\sigma_\theta^* = \frac{1}{r^{*2}} [\int_{r_{g^*}}^{r^*} T^* r^* dr^* - T^* r^{*2}] \tag{22}$$

$$\sigma_z^* = -T^* \tag{23}$$

The equivalent stress can be written as [22]:

$$\sigma_e = \sqrt{\frac{1}{2}\left[(\sigma_r - \sigma_\theta)^2 + (\sigma_r - \sigma_z)^2 + (\sigma_z - \sigma_\theta)^2\right]} \tag{24}$$

or dimensionless stress becomes:

$$\sigma_e^* = \sqrt{\frac{1}{2}\left[(\sigma_r^* - \sigma_\theta^*)^2 + (\sigma_r^* - \sigma_z^*)^2 + (\sigma_z^* - \sigma_\theta^*)^2\right]} \tag{25}$$

It should be noted that thermo-mechanical coupling between the temperature and stress fields is omitted, since it is reported to be negligibly small [22].

3 NUMERICAL SOLUTION AND PULSE PROFILES

A set of governing equations 5, 6 and 7 are solved numerically. The solid and liquid heating, equation 5 is considered, equation 6 is employed for the mushy zone at solid-liquid interface while equation 7 is used for the mushy zone at liquid-vapor interface. To discretize the governing equations, a control volume approach is introduced. The details of the numerical scheme are given in [23]. To compute the equations discretized for temperature field and relative positions of solid-liquid and liquid- vapor interface, an explicit scheme (a time marching scheme) is employed. The stability criteria due to time increment are considered for a stable solution; therefore, the time increment is limited by:

$\left(\frac{2k}{\rho c_p \Delta r^2} + \frac{2k}{\rho c_p \Delta z^2}\right) \Delta t \leq 1$

The calculation domain is divided into grids and grid independence tests are performed for different grid size and their orientations. A non-uniform grid with 500×500 mesh points is employed after securing the grid independence, i.e. the grid size resulting

in grid independent solution is selected, which is 500×500. In this case, the finer grids are located near the irradiated spot center in the vicinity of the surface and the coarse grids are set as the distance increases towards the bulk of substrate material. Time increment satisfying the stability criteria for the finest grid is calculated as 5×10^{-13} s. A computer program based on explicit scheme is developed to compute the temperature field. In stress calculations the resulted temperature field is employed for performing the numerical integration.

The material properties corresponding to stainless steel and pulse intensity used in the simulations are given in Tables 1 and 2, respectively .

4 RESULTS AND DISCUSSION

The numerical simulation of laser pulse heating of steel is carried out. The phase change processes including melting and evaporation are incorporated in the analysis. The temperature field in the substrate material and thermal stresses developed in the solid phase of the substrate material are computed for time exponentially varying laser heating pulse. The laser pulse and material properties used in the simulations are given in Tables 1 and 2.

Figure (2) shows the dimensionless temperature contours inside the substrate material for two pulse parameters $\left(\frac{\beta}{\gamma} = \frac{1}{2} \text{ and } \frac{\beta}{\gamma} = \frac{1}{4}\right)$. It should be noted that the ratio of $\frac{\beta}{\gamma}$ is limited with the data given in Table 2.

Temperature Field:

Temperature contour beyond 0.12 is not plotted, since the value 0.12 corresponding to the evaporation temperature, i.e. the empty space in the figure indicates the shape of the cavity generated after the evaporation process. The depth of the cavity extends further inside the substrate material for $\frac{\beta}{\gamma} = \frac{1}{4}$ despite the fact that peak power intensity for both pulses are the same (figure (3)). In this case, the pulse intensity rise rapidly and attains high values for $\frac{\beta}{\gamma} = \frac{1}{4}$ as compared to that corresponding to $\frac{\beta}{\gamma} = \frac{1}{2}$. The rapid rise of the pulse intensity enhances the heating process during the early heating period. The size of the cavity at the surface of the substrate material is in the order of $40\mu m$ $(r^* = 2500)$, after about 0.6 ns heating pulse $(t^* = 6.1)$, which is almost the same as the irradiated spot size. Moreover, for pulse parameter $\frac{\beta}{\gamma} = \frac{1}{2}$, this reduces slightly.

Figure (4.a) shows temperature profiles inside the substrate material at r-axis location is zero $(r^* = 0)$ for different heating periods. The temperature profiles up to the evaporation temperature are shown. Temperature profiles reduces sharply in the liquid region and the decay is almost gradual in the solid region. This can also be seen from figure (4.b), in which temperature gradient $\left(\frac{\partial T}{\partial r}\right)$ is shown inside the substrate material. Temperature gradient changes sharply in the melt region $(.07 < T^* < .12)$ while change is relatively gradual in the solid region $(T^* < .07)$. The region of melting is evident from $\frac{\partial T}{\partial r}$ curve, in which case, $\frac{\partial T}{\partial r}$ changes at the point of phase change. Moreover, $\frac{\partial T}{\partial r}$ reduces to reach its minimum before it increases. Although z-axis location $(z^* = 6.2)$ is beyond

the absorption depth, the heat diffusion across the liquid-solid interface increases considerably the internal energy gain of the substrate material. Consequently temperature gradient attains high values. As the depth increases further, the temperature gradient increases gradually. This occurs because of the diffusional energy transport, i.e. in the solid next to the melt region, large temperature gradient accelerates the diffusional energy transport from this region to bulk of the substrate material; however, as the depth below the surface increases further, temperature gradient becomes less and diffusional energy transport towards the solid bulk reduces. This is more pronounced in the early heating period. As the heating period progresses ($t^* > 4.5$), the decay rate of temperature profiles becomes almost same.

Figure (5.a) shows the dimensionless temperature distribution along the radial direction at z-axis location is zero ($z^* = 0$) for different heating periods. The widths of evaporated, melted and solid heated zones are evident. This can also be seen from figure (5.b), in which temperature gradient in the radial direction $\left(\frac{\partial T^*}{\partial r^*}\right)$ is shown. The temperature gradient reduces sharply in the melt region and decay of gradient reduces as the distance from the irradiated spot center increases towards the edge of the heated spot. Moreover, the decay of the temperature in the radial direction did not follow the pulse intensity profile in the same direction, i.e. temperature decay rapidly towards the edge of the heated spot. The variation of temperature distribution in the radial direction with heating period is not considerable. This is because of the time exponentially varying pulse, in which case, peak intensity does not alter considerably within the heating period considered (figure (3)).

Figure (6) shows temporal variation of surface temperatures obtained from enthalpy and energy methods for constant and variable properties for comparison. Moreover, temperature profiles obtained from two-dimensional energy method for constant and variable properties are also shown. It should be noted that the constant properties correspond to the room temperature properties of the substrate material. Since the analysis related to the enthalpy method is one-dimensional, temperature profiles obtained from one-dimensional analysis of energy and enthalpy methods are presented. It can be seen that the results obtained from enthalpy and present model are in good agreement. In addition, temperature profile obtained from two-dimensional model for constant properties becomes similar to that corresponding to one-dimensional heating situation. This indicates that the radial heat conduction in the surface vicinity is considerably smaller than the heat conduction in the axial direction, particularly for constant properties case. Moreover, the effect of variable properties on temperature profiles are evident from temperature predictions of two-dimensional energy methods. In this case, the rate of temperature rise becomes less for the variable properties case, i.e. the specific heat capacity and thermal conductivity reduce with increasing temperature (Table 1), which in turn alters the heat diffusion rates inside the substrate material.

Thermal Stress Field:

Figure (7) shows the dimensionless tangential stress component along the axial direction as dimensionless heating periods are variable. Tangential stress component is compressive, provided that stress level at the melt boundary is zero, i.e. free stress

condition is set at melt surface in the simulations. The magnitude of stress component increases sharply as the distance from the melt surface, reaching its maximum before decreasing sharply to at some depth below the surface. The behavior of stress component in the axial direction is because of the temperature gradient, in which case, the magnitude of temperature gradient in this region decays sharply. As the heating period progresses, the magnitude of maximum stress remains the same, however, its location moves away from the center of the heated spot. This occurs because of the advancement of the melt surface in the axial direction as the heating period progresses. Moreover, the behavior of tangential stress gradients corresponding to different heating periods is almost same. This is due to the surface temperature gradient behavior with time.

Figure (8) shows the dimensionless tangential stress component along the radial distance as the dimensionless heating period is variable. The tangential stress component is compressive in the region close to the irradiated spot center and it becomes tensile as the distance from the spot center increases towards the edge. This is because of the thermal strain generated in this region, i.e. thermal expansion results in contraction in the region close to the irradiated spot center. The magnitude of stress component increases sharply to reach its maximum in the region below the melt zone and it reduces sharply to zero as the radial distance increases. Moreover, increasing the radial distance further towards the solid bulk results in increase in the stress component, provided that the stress component becomes tensile. The level and stress profile remain almost same with time.

Figure (9) shows the dimensionless radial stress component along the radial-axis as dimensionless heating periods are variable. Radial stress component is compressive, which is because of the thermal strain developed in the radial direction. The magnitude of stress component increases sharply to reach its peak and decays gradually as the distance in the radial direction increases away from the irradiated spot center. The location of maximum stress component remains the same for all the heating periods considered, however, its magnitude increases with progressing heating period. Moreover, stress gradient increases in the region close to the irradiated spot center as the heating progresses. This occurs because of the radial temperature gradient, which increases slightly in this region with progressing heating period.

Figure (10) shows the 3-dimensional plot of dimensionless equivalent stress for two dimensionless heating periods. The equivalent stress level varies considerably along the axial and radial directions. Figure (11) shows the dimensionless equivalent stress along the radial distance as heating periods are variable. The magnitude of stress increases sharply to reach its maximum in the region next to the melt zone. As the radial distance increases away from the melt surface stress level reduces to reach minimum. As the distance increases further, the stress level increases reaching its second peak, provided that the magnitude of the second peak is less than that corresponding to the first peak. Moreover, the rise of second peak is gradual while the rise of first peak is sharp. The generation of second peak is because of the radial component of the tangential stress, which becomes tensile in this region. The influence of heating period on the equivalent stress is more pronounced for the second stress peak. In this case, the magnitude of stress level reduces as the heating period progresses.

Figure (12) shows the dimensionless equivalent stress along the axial direction as

dimensionless heating period is variable. equivalent stress increases sharply to reach its maximum in the region next to the melt surface. As the radial distance increases further towards the irradiated spot edge it decays gradually. This occurs because of the tangential stress component (figure (8)), in which case, behaviors of equivalent and tangential stress levels in the radial direction are almost identical. The maximum equivalent stress moves towards the solid bulk as the heating period progresses, provided that the stress gradients during rise and fall do not change much for different heating periods. The change of maximum stress location is because of; i) advancing of melt surface towards the solid bulk with progressing of heating period, and ii) temperature profile next to the melt zone does not alter considerably for different heating periods.

5 CONCLUSIONS

The non-conduction limited laser heating of steel is considered. Time exponentially varying pulse is employed to resemble the actual heating pulse. The Fourier heating model is used when formulating the energy transport while thermal stress analysis is introduced when formulating the stress field due to a resulting temperature field. A numerical method employing a control volume approach is used to discretize the governing equations. It is found that the pulse parameter $\left(\frac{\beta}{\gamma}\right)$ has a considerable effect on the temperature profile, in this case, as $\frac{\beta}{\gamma}$ reduces, the size of the evaporated zone increases. It should be noted that the magnitude of β and γ defines the length of the laser pulse intensity; in which case, small values of β and γ result in short pulses. In practical application of laser processing, the temporal variation of a laser pulse follows almost similar to the function $[\exp(-\beta t) - \exp(-\gamma t)]$. In this case, varying $\frac{\beta}{\gamma}$ modifies the laser pulse shape. Consequently, early rise of the laser pulse ($\frac{\beta}{\gamma} = \frac{1}{2}$) has advantage of creating the deep cavities. The equivalent stress increases significantly in the region next to the melt zone. The specific conclusions derived from the present study can be listed as follows:

1. Temperature gradient attains high values in the melt zone and it reduces gradually as the distance from the surface increases further towards the bulk zone. The effect of heating period on the temperature profile in the axial direction is significant while its counterpart corresponding to radial direction is not notable. This indicates that the energy conducted in the radial direction is less as compared to that occurring in the axial direction.

2. Tangential stress component in the axial direction is compressive. The stress component increases sharply reaching its maximum in the region next to the melt surface. As the heating period progresses, the location of peak stress moves away from the irradiated center similar to the melt surface advancing in the same direction. Tangential stress component in the radial direction is compressive in the region close to the melt surface and it becomes tensile as the distance increases towards the edge of the irradiated spot in the radial direction. This occurs because of the thermal strain developed in the radial direction due to temperature gradient in this direction.

3. Radial stress component is compressive along the radial direction. Stress com-

ponent increases sharply in the region close the melt surface. The decay of the stress component from its maximum level is gradual in the radial direction. The maximum magnitude of stress level increases with progressing heating period while the location of maximum stress level remains same in the radial direction.

4. Equivalent stress increases sharply along the axial direction in the region next to the melt surface. The location of maximum stress level moves away from the melt surface as heating period progresses. Equivalent stress has two peaks in the radial direction, provided the magnitude of second peak decreases with heating period. The locations of equivalent stress peaks do not vary with heating period.

References

1 - Ready J. F.,"Effects due to absorption of laser radiation", J. Appl. Phys., Vol.36, pp. 462-470, 1963.

2 - Simon G. Grotzke U. and Kross J.,"Analysis of heat conduction in deep penetration welding with a time-modulated laser beam", J. Phys. D: Appl. Phys., Vol.26, pp.862-869, 1993.

3 - Lu Y.,"Square-shaped temperature distribution induced by a Gaussian-shaped laser beam", Appl. Surf. Science, Vol. 81, pp. 357-364, 1994.

4 - Al-Adawi M.K., Abel-Naby M.A. and Shalaby S.,"Laser heating of a two layer system with constant surface absorption: an exact solution", Int. J. Heat and Mass Transfer, Vol.38, No.5, pp.947-952, 1995.

5 - Basu B. and Date A.W.,"Numerical study of steady state and transient laser melting problems - 1. characteristics of flow field and heat transfer", Int, J, Heat Mass Transfer, Vol. 33, pp. 1149-1163, 1990.

6 - Wei P.S. and Ho J.Y.,"Energy considerations in high-energy beam drilling", Int. J. Heat and Mass Transfer, Vol. 33, pp. 2207-2217, 1990.

7 - Bang S.Y. and Modest M.F.,"Multiple reflection effects on evaporative cutting with a moving cw laser", ASME, J. Heat Transfer, Vol. 113, pp. 663-669, 1991.

8 - Kim W. and Sim B.,"Study of thermal behavior and fluid flow during laser surface heating of alloys", Numerical Heat Transfer part a, Vol. 31, pp. 703-723, 1997.

9 - Yilbas B.S. and Shuja S.Z.,"Heat transfer analysis of laser heated surfaces- conduction limited case", Applied Surface Science, Vol.108, pp.167-175, 1997.

10 - Yilbas B.S. and Al-Garni A.Z.,"Some aspects of laser heating of engineering materials", J. Laser Applications, Vol 8, pp.197-204, 1996.

11 - Yilbas B.S., Sahin A., and Davies R.,"Laser heating mechanism including evaporation process initiating the laser drilling", Int.J. , Mach. Tools and Manufact. Vol.35, No.7, pp.1047-1062, 1995.

12 - Paek U. and Gagliano F.P. , Thermal analysis of laser drilling - IEEE J. Quantum Electronics, Vol. 8, pp. 112-119, 1972.

13 - Elperin, T. and Rudin, G.,"Thermo-elasticity problem for a multilayer coating-substrate assembly irradiated by a laser beam", Int. Comm. Heat Mass Transfer, Vol. 23, pp. 133-142, 1996.

14 - Wang, H.G., Guan, Y.H., Chen, T.L. and Zhang, J.T., " A study of thermal stresses during laser quenching", J. Materials Proc. Tech., Vol. 63, pp. 550-553, 1997.

15 - Li, K. and Sheng, P., "Plane stress model for fracture of ceramics during laser cutting", Int. J. Mach. Tools mfg., Vol. 35, pp. 1493-1506, 1995.

16 - Dain, Y., Kapadia, P.D. and Dowden, J.M., " The distortion gap width and stresses in laser welding of thin elastic plates", J. Phys. D: Appl. Phys., Vol. 32, pp. 168-175, 1999.

17 - Yilbas, B.S., Sami, M., and Shuja, S.Z., "Laser-induced thermal stresses on steel surface", Optics and Lasers in Engineering., Vol. 30, pp. 25-37, 1998.

18 - B.S. Yilbas, Analytical solution for time unsteady laser pulse heating of semi-infinite solid - Int. J. Mechanical Sciences, Vol.39, No.6, pp.671-682, 1997.

19 -Yilbas B.S. and Shuja S.Z.,"Laser short-pulse heating of surfaces", J. Phys. D: Appl. Phys., 32, 1947-1954, 1999.

20 - Yilbas B.S. and Shuja S.Z.,"One equation, two-equation and kinetic theory: laser pulse heating), Jap. J. Appl. Physics, Vol. 39, pp. 4018-4027, 2000.

21 - Ozisik M.N.,"Heat Conduction", 2 nd ed., John Wiley and Sons, pp. 423-430, New York, 1993.

22 - S. P. Timenshenko and J.N. Goodier, Theory of elasticity, 3rd ed., pp.476-484, McGraw-Hill Book Comp., Singapore, 1984.

23 - Smith G.D.,"Numerical solution of partial differential equations: finite difference methods", 3rd edn, Clarendon Press, Oxford, 1985

24 - Incorpera F.P. and De Witt D.P.,"Fundamentals of heat and mass transfer", 2nd ed.,pp. 756, 1985.

6 Nomenclature

a : Gaussian parameter (m)

a^* : Dimensionless Gaussian parameter $(a\delta)$

c_p : Specific heat capacity $\left(\frac{J}{kgK}\right)$

E : Elastic modulus $\left(\frac{N}{m^2}\right)$

I_o : Laser peak power intensity $\left(\frac{W}{m^2}\right)$

k : Thermal conductivity $\left(\frac{W}{mK}\right)$

L_b : Latent heat of evaporation $\left(\frac{J}{kg}\right)$

L_m : Latent heat of melting $\left(\frac{J}{kg}\right)$

T : Temperature (^oC)

r : Radial distance (m)

r_g :Distance of solid-liquid interface from axis of symmetry (m)

r_g^* :Dimensionless distance of solid-liquid interface from axis of symmetry $(r_g\delta)$

r^* : Dimensionless radial distance $(r\delta)$

r_f : Reflection coefficient

S_o : Source term (W)

T^* : Dimensionless temperature $\left(\frac{Tk\delta}{I_o}\right)$

T_b : Boiling temperature (^oC)

T_m : Melting temperature (^oC)

T_o : Initial temperature (^oC)
t : Time (s)
t^* : Dimensionless time $(\alpha\delta^2 t)$
ΔU : Energy content of differential volume (J)
Δu : Energy content per unit volume $\left(\frac{J}{m^3}\right)$
dV : Differential volume (m^3)
x_b : Mass fraction of vapor
x_m : Mass fraction of melt phase
z : Axial distance (m)
z^* : Dimensionless axial distance $(z\delta)$

Greek Symbols:

α : Thermal diffusivity $\left(\frac{m^2}{s}\right)$
α_T : Coefficient of thermal expansion (K^{-1})
δ : Absorption depth(m^{-1})
ε_r : Radial strain
ε_z : Axial strain
ε_θ : Tangential strain
ν : Poisson's ratio
σ_e : Equivalent stress $\left(\frac{N}{m^2}\right)$
σ_r : Radial stress $\left(\frac{N}{m^2}\right)$
σ_z : Axial stress $\left(\frac{N}{m^2}\right)$
σ_θ : Tangential stress $\left(\frac{N}{m^2}\right)$
σ_e^* : Dimensionless equivalent stress $\left(\sigma_e \left[\frac{1-\nu}{\alpha_T E}\right] \left[\frac{k\delta}{I_o(1-r_f)}\right]\right)$
σ_r^* : Dimensionless radial stress $\left(\sigma_r \left[\frac{1-\nu}{\alpha_T E}\right] \left[\frac{k\delta}{I_o(1-r_f)}\right]\right)$
σ_z^* : Dimensionless axial stress $\left(\sigma_z \left[\frac{1-\nu}{\alpha_T E}\right] \left[\frac{k\delta}{I_o(1-r_f)}\right]\right)$
σ_θ^* : Dimensionless tangential stress $\left(\sigma_\theta \left[\frac{1-\nu}{\alpha_T E}\right] \left[\frac{k\delta}{I_o(1-r_f)}\right]\right)$
φ : Stress function $\left(\frac{N}{m^3}\right)$

Appendix 1 - Enthalpy Method:

The one-dimensional enthalpy equation governing the energy transport due to conduction with the heat source inside the substrate material can be written as [21]:

$$\rho\frac{\partial H}{\partial t} = k\frac{\partial^2 T}{\partial z^2} + S_o$$

where the source term is:

$$S_o = I_o\delta\left(1 - r_f\right)\exp\left(-\delta z\right)$$

The appropriate boundary conditions for the phase change can be written as [16]:

$$T = \begin{cases} \frac{H}{c_p} & H < c_p T_m \\ T_m & c_p T_m \leq H \leq c_p T_m + L_m \\ \frac{H - L_m}{c_p} + T_o & c_p T_m + L_m < H < c_p T_b + L_m \\ T_b & c_p T_b + L_m \leq H \leq c_p T_b + L_m + L_b \end{cases}$$

The solution of enthalpy equation is obtained numerically to compare with the one-dimensional energy method predictions for the same substrate material and pulse properties.

	δ (1/m)	ρ (kg/m^3)	Cp $Cp_m = Cp$ at $T = T_m$ (J/KgK)	k $k_m = k$ at $T = T_m$ (W/mK)	T_m (K)
Constant Properties	6.16×10^7	7836	330	52	1810
Variable Properties	6.16×10^7		24.558+1.223×T -0.37693×10^{-3}T^2	64.102-0.04803T +1.518×10^{-5}T^2	
L_m (J/kg)	L_b (J/kg)	E (GPa)	ν	$\alpha_T \times10^{-6}$ (1/K)	T_b (K)
2.4×10^5	6.26×10^6	11.7	0.3	217.96	3030

Table 1: Properties of substrate material used in the computation [24]

Pulse Intensity (W/m^2)	Gaussian Parameter a (1/m)	Heating period (ns)	β (1/s)	γ (1/s)
7×10^{12}	3.266×10^3	$0 - 8$	0.5×10^9	1×10^9-2×10^9

Table 2: Pulse properties used in the computation.

Acknowledgments

The authors acknowledge the support of King Fahd University of Petroleum and Minerals. Dhahran, Saudi Arabia for this work.

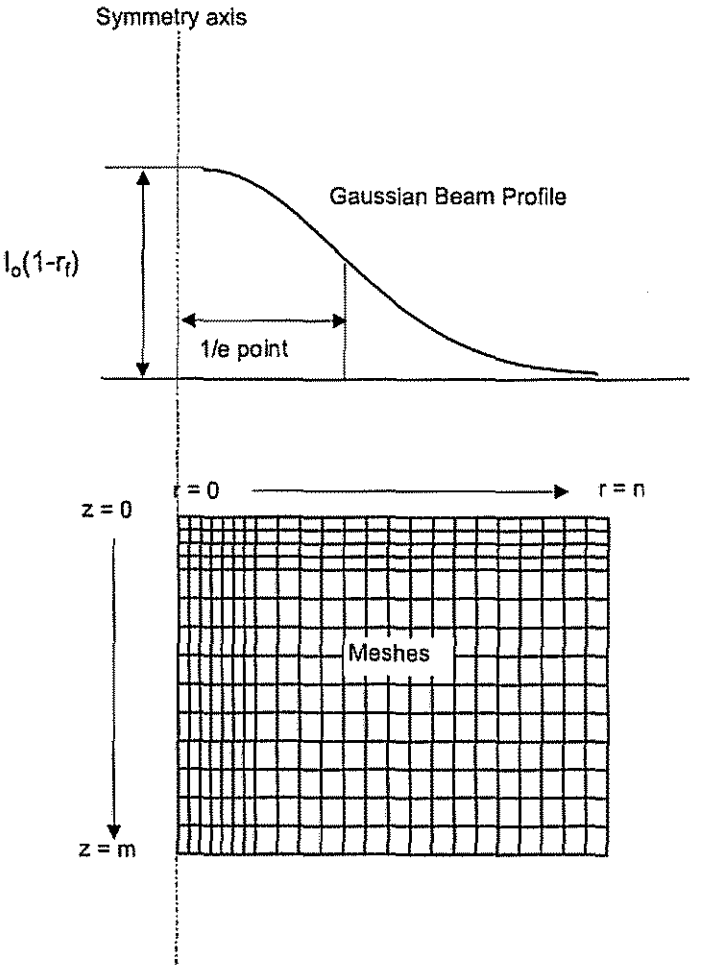

Fig. 1.a Schematic view of laser beam profile and mesh points (n = 480 and m = 500).

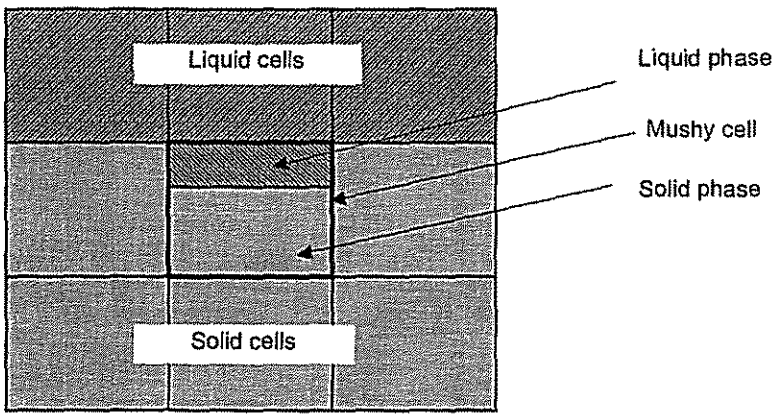

Fig. 1.b Schematic view of a mushy cell.

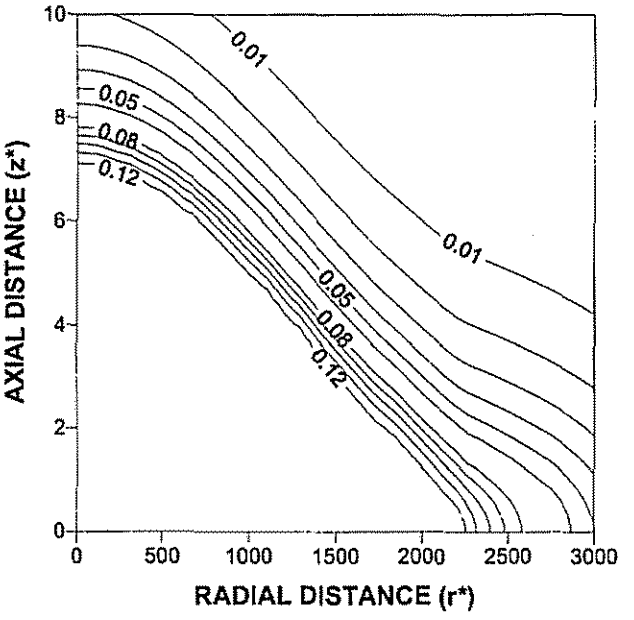

$\beta/\gamma = 1/2$

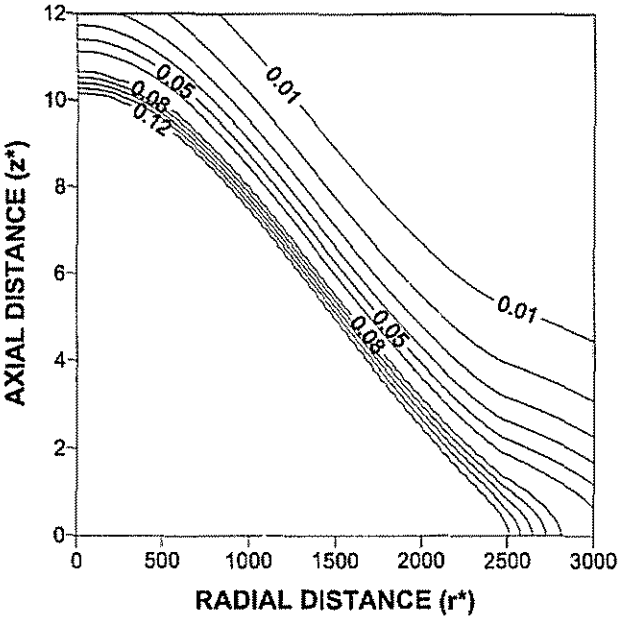

$\beta/\gamma = 1/4$

Fig. 2. Temperature contours at Time = 6.1

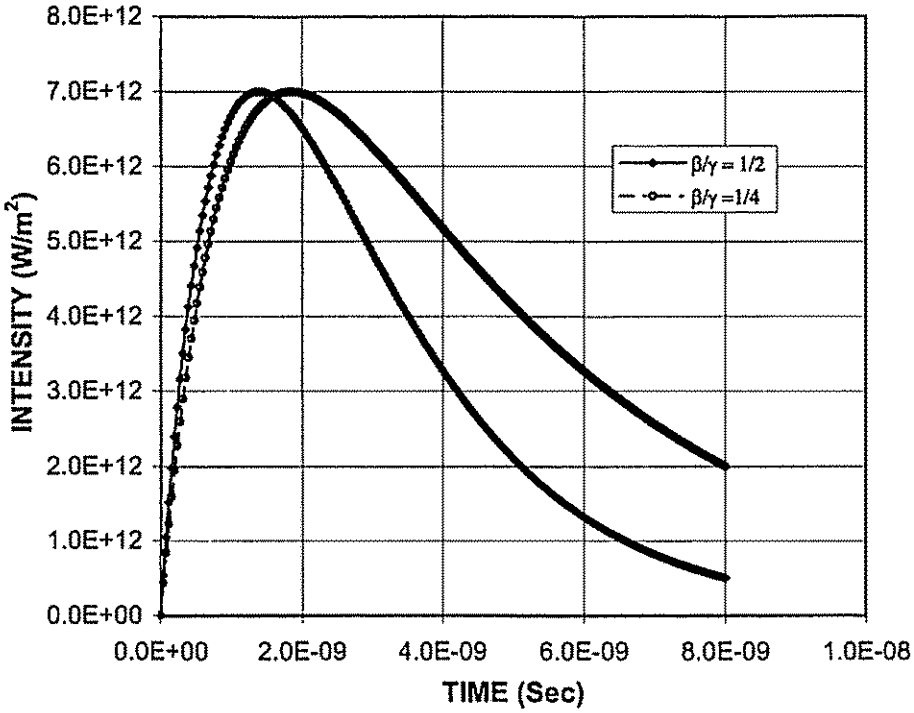

Fig. 3 Power intensity distribution with time for time exponentially varing pulse.

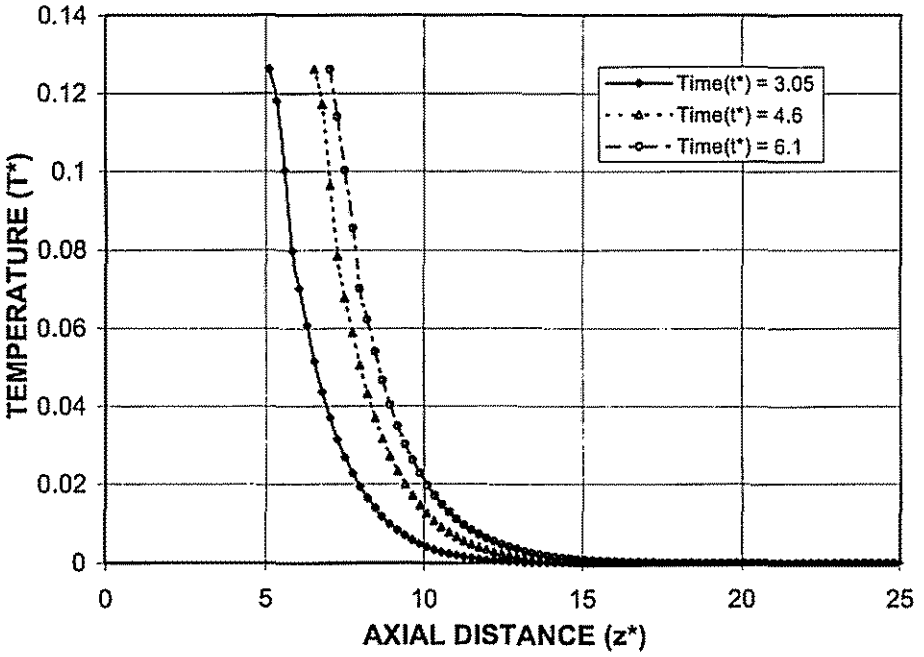

Fig. 4.a Variation of dimensionless temperature along dimensionless axial distance at radial location r* = 0 for different heating periods.

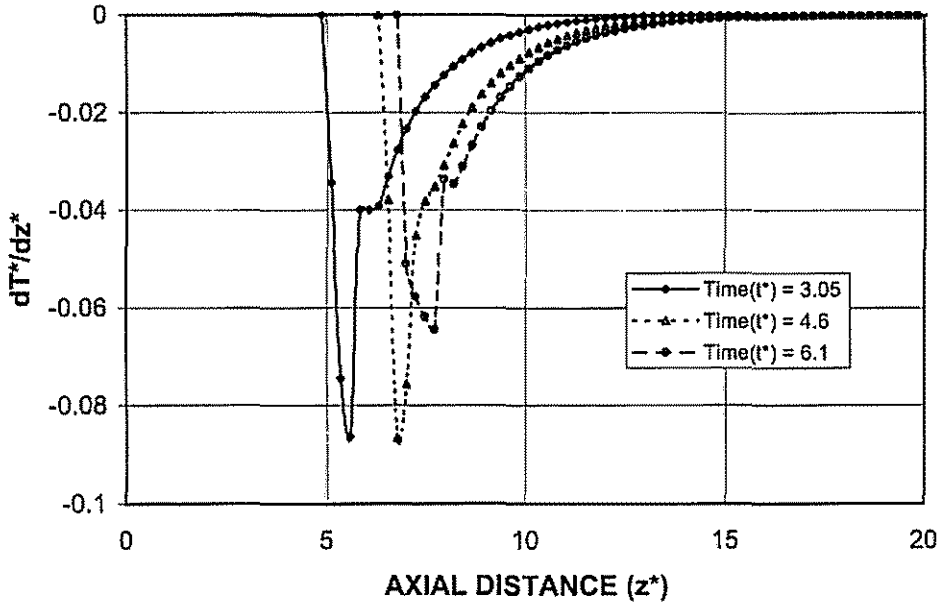

Fig. 4.b Variation of dimensionless temperature gardient along dimensionless axial distance at radial location r* = 0 for different heating periods.

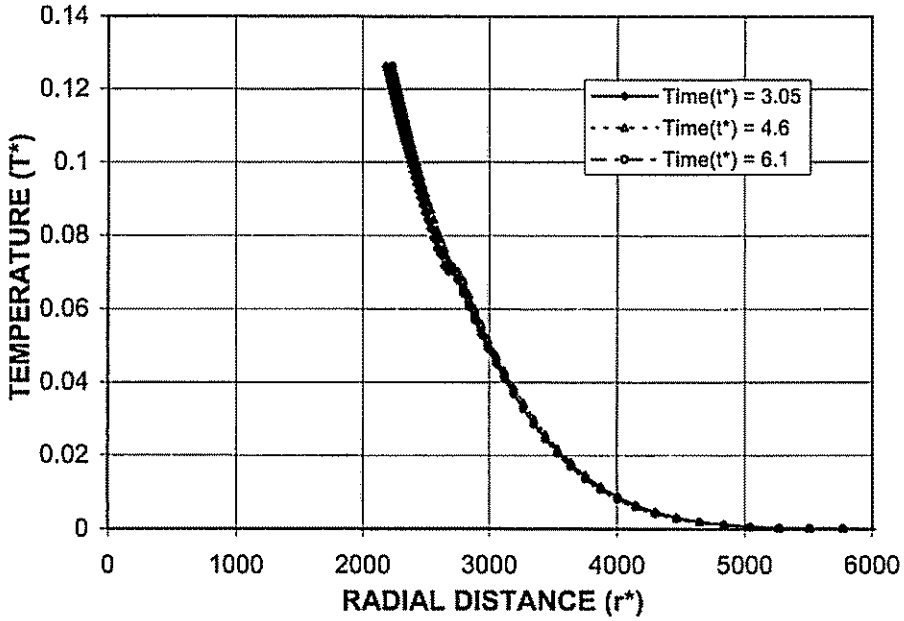

Fig. 5a Variation of dimentionless temperature along dimensionless radial distance at axial location z* = 0 for different heating periods.

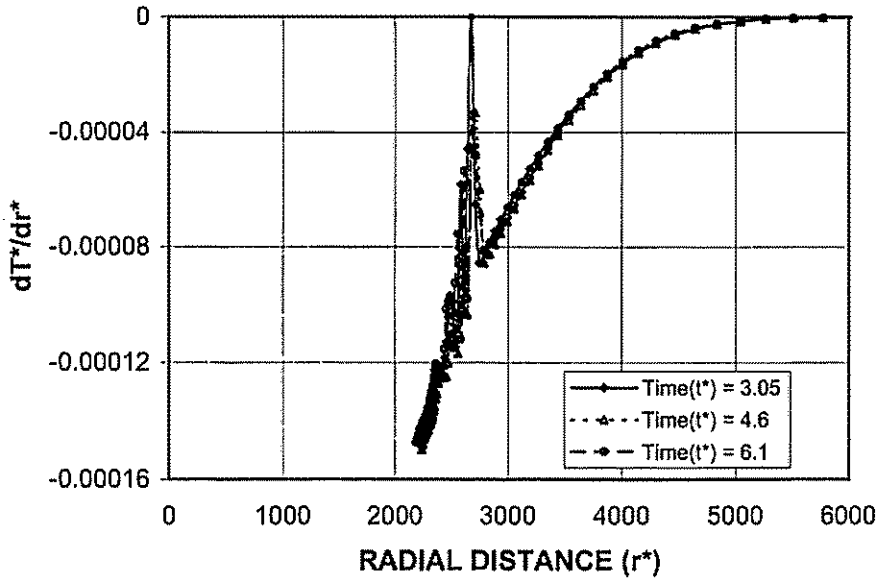

Fig. 5b Variation of dimentionless temperature gradient along dimensionless radial distance at axial location z* = 0 for different heating periods.

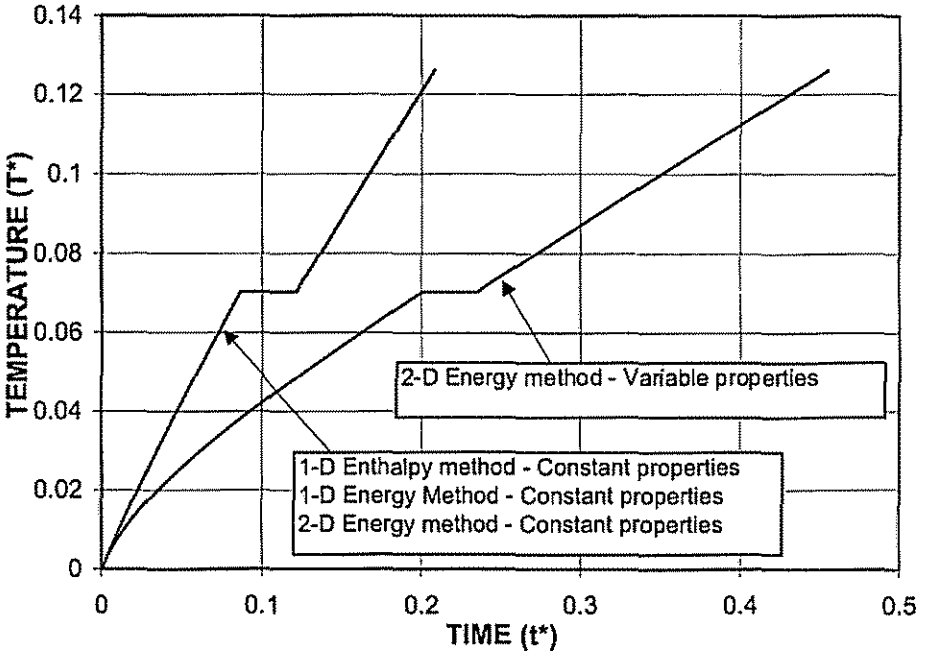

Fig. 6 Temporal variation of dimensionless surface temperature at axial and radial location of $z^* = 0$: $r^* = 0$ and obtained from energy and enthalpy methods for constant properties. The constant and variable properties cases corresponding to two-dimensional energy method is also presented for comparison reason.

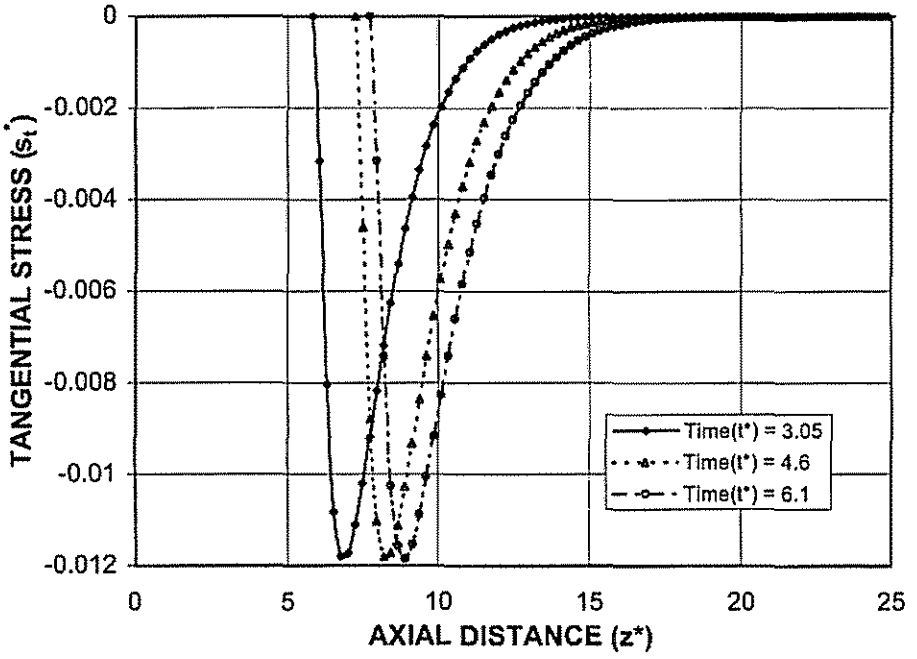

Fig. 7 Variation of dimensionless tangential stress along dimensionless axial distance at radial location $r^* = 0$ for different heating periods.

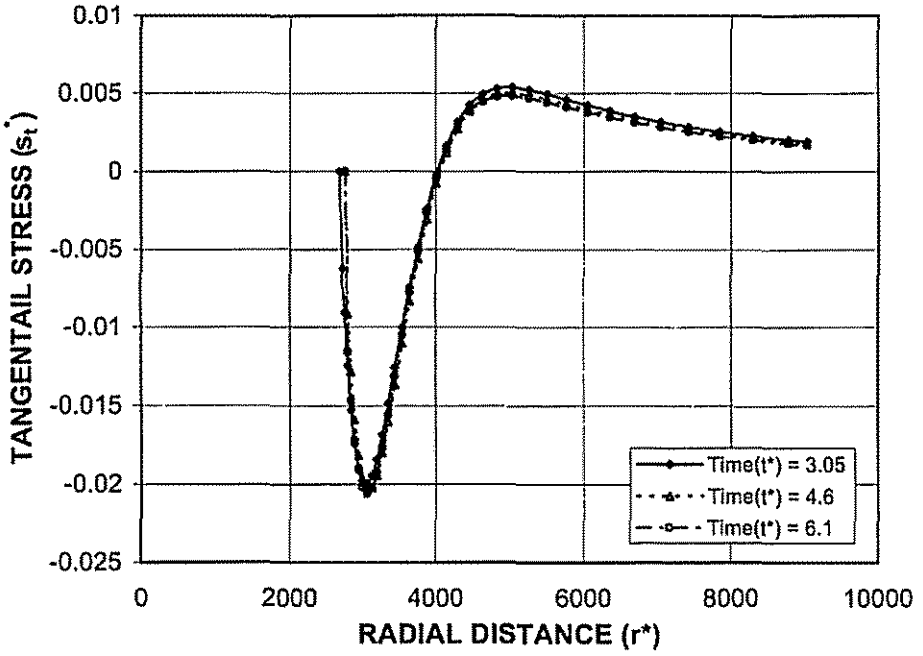

Fig. 8 Variation of dimensionless tangential stress along dimensionless radial distance at axial location $z^* = 0$ for different heating periods.

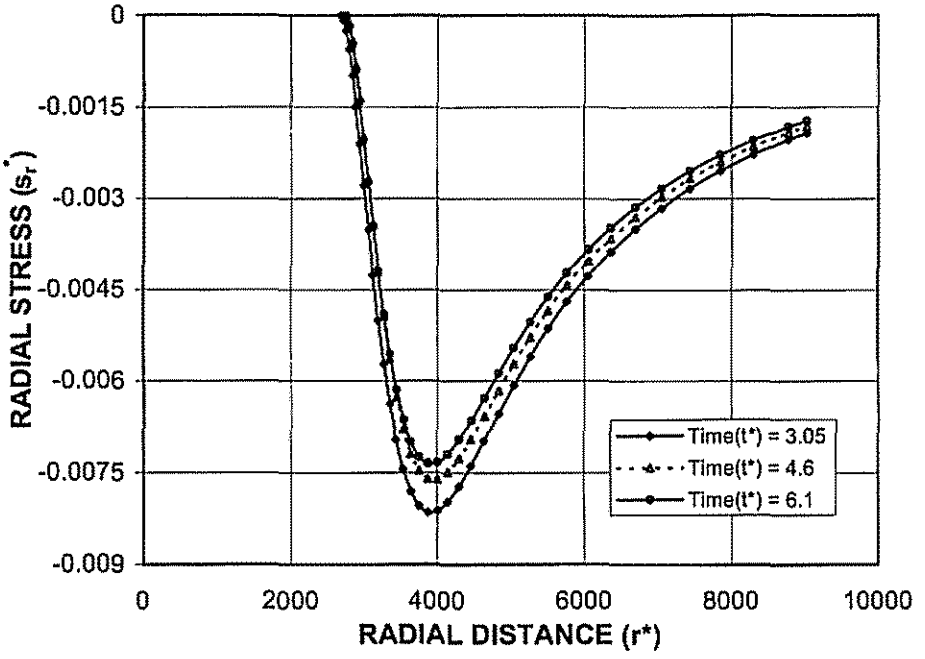

Fig. 9 Variation of dimensionless radial stress along dimensionless radial distance at axial location $z^* = 0$ for different heating periods.

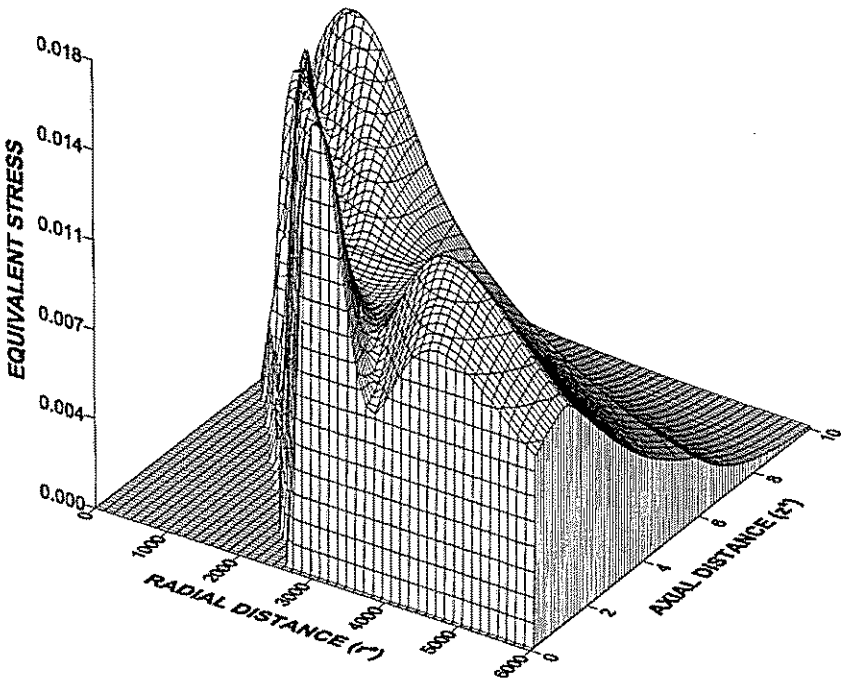

Time (t*) = 3.05

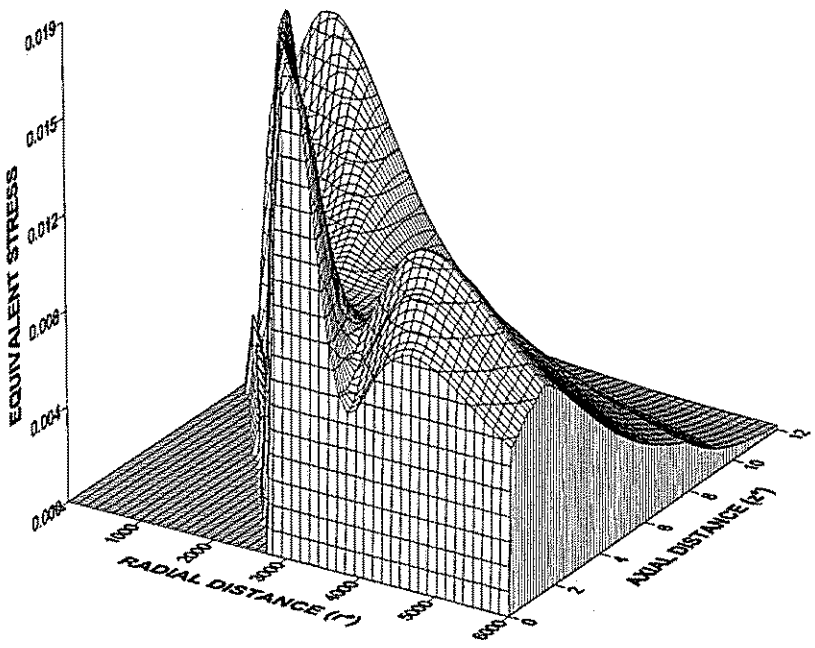

Time (t*) = 6.1

Fig. 10. Equivalent stress surface plot

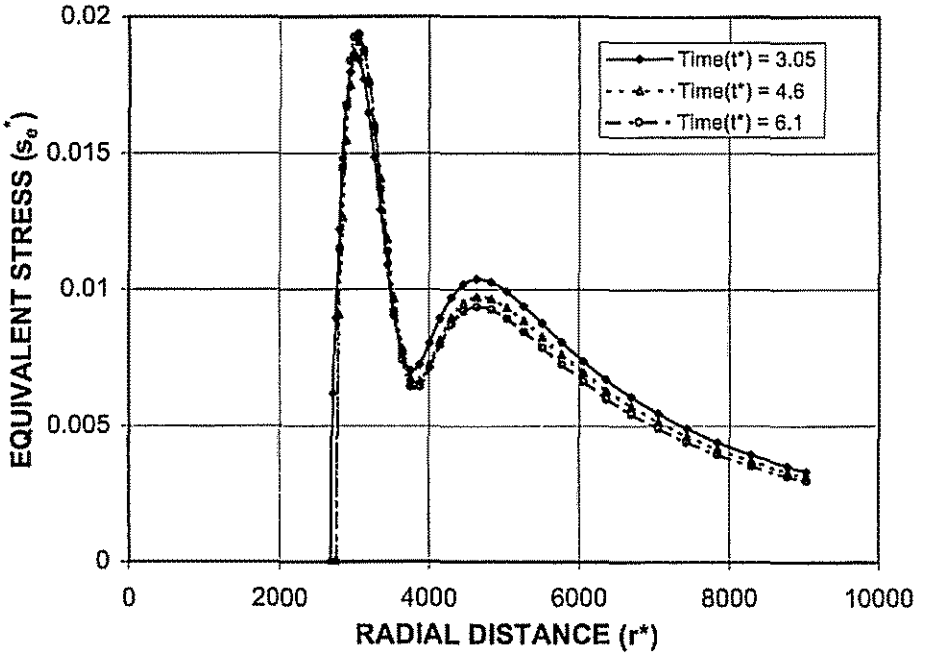

Fig. 11 Variation of dimensionless equivalent stress along dimensionless radial distance at axial location $z^* = 0$ for different heating periods.

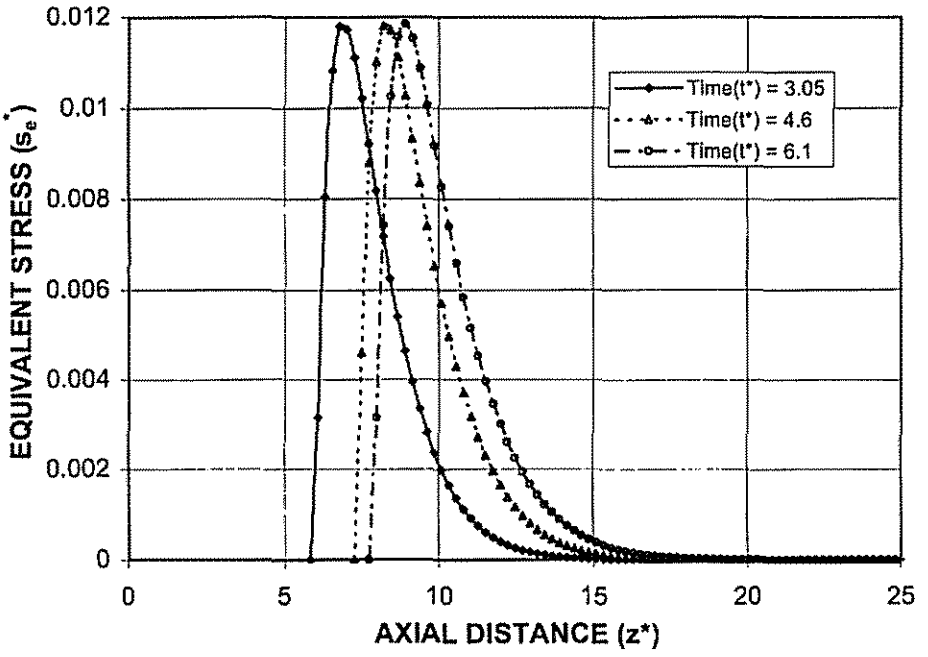

Fig. 12 Variation of dimensionless equivalent stress along dimensionless axial direction at radial location $r^* = 0$ for different heating periods.